Subtropical Cirrus Properties Derived from GSFC Scanning Raman Lidar Measurements during CAMEX 3

D. N. Whiteman, Z. Wang, B. Demoz

Abstract

The NASA/GSFC Scanning Raman Lidar (SRL) was stationed on Andros Island, Bahamas for the third Convection and Moisture Experiment (CAMEX 3) held in August – September, 1998 and acquired an extensive set of water vapor and cirrus cloud measurements (Whiteman et. al., 2001). The cirrus data studied here have been segmented by generating mechanism. Distinct differences in the optical properties of the clouds are found when the cirrus are hurricane-induced versus thunderstorm-induced. Relationships of cirrus cloud optical depth, mean cloud temperature, and layer mean extinction-to-backscatter ratio (S) are presented and compared with mid-latitude and tropical results. Hurricane-induced cirrus clouds are found to generally possess lower values of S than thunderstorm induced clouds. Comparison of these measurements of S are made with other studies revealing at times large differences in the measurements. Given that S is a required parameter for space-based retrievals of cloud optical depth using backscatter lidar, these large differences in S measurements present difficulties for space-based retrievals of cirrus cloud extinction and optical depth.

Introduction

Cirrus clouds affect the earth's radiation budget strongly by influencing both the greenhouse effect and planetary albedo (Liou 1986) and can create errors in satellite retrievals. The study of McFarquher et al. (2000) showed that tropopause tropical cirrus clouds with optical depths of 0.01 have corresponding heating rates and cloud radiative forcing of 1.66 K day^{-1} and 1.6 W m^{-2}, respectively. Cloud climatology studies based on SAGE II observations (Wang et.al., 1996) have indicated frequencies of sub-visual cirrus (optical depths below ~0.03) near the tropical tropopause of up to 70% indicating that the radiative effects of cirrus clouds are very large in tropical locations. Furthermore, the radiative effects of optically thin cirrus clouds can introduce errors in satellite remote sensing of tropospheric aerosols (Gao et. al., 2002) and water vapor (Whiteman, et al. 2001). Space-based lidar offers a great potential for acquiring accurate global statistics on cloud heights and optical depths. However, due to the influence of multiple scattering on space-based cloud measurements, the retrieval of cirrus cloud optical depth will likely require an accurate parameterization of the extinction to backscatter ratio for cirrus clouds.

Midlatitude cirrus cloud properties have been extensively studied using lidar, cloud radar and radiometers (Platt et al. 1987, Mace et al. 2001, Sassen and Comstock 2001, Wang and Sassen 2002, Sakai et. al., 2003) but corresponding measurements in tropical or sub-tropical areas are more limited (Sassen et al., 2000; Platt et al. 1998; Comstock et al. 2002) and none of those studies has been with a Raman lidar. During July-September, 1998 the NASA/GSFC Scanning Raman Lidar (SRL) was stationed on Andros Island (24.7N, -77.75W) in the Bahamas as a part of the third Convection and Moisture Experiment (CAMEX 3). Though the main goal of the SRL participation in CAMEX-3 was to acquire detailed water vapor measurements during hurricane season, the system also provided high quality measurements of cirrus clouds. Optical properties

of sub-tropical cirrus derived from approximately 220 hours of SRL cloud measurements are studied here and compared with other measurements from the mid-latitudes and tropics.

The NASA/GSFC Scanning Raman Lidar (SRL)

The SRL is a mobile lidar system designed to detect light backscattered at the laser wavelength by molecules and aerosols as well as Raman-backscattered light from water vapor, nitrogen, and oxygen molecules. The measurements presented here were acquired using a XeF excimer laser with output power between 12-20W, a 0.76 m telescope, a full-aperture scanning mirror and 2 photomultipliers for each sensed wavelength. More details on the Raman Lidar technique and on the configuration of the SRL at the time of the CAMEX-3 campaign can be found in Whiteman et.al, 1992, Whiteman et. al., (2001) and Whiteman and Melfi (1999). The SRL measurements analyzed here were acquired at night and ten-minute average quantities were used in the calculation of all data products.

Data Analysis Techniques

Many of the techniques used to analyze the data are described fully in Whiteman et. al., (2001) and Whiteman 2003 a,b so only brief descriptions of data analysis techniques will be provided here. Cloud optical depth is calculated using a Beer's Law approach where the total attenuation of the vibrational Raman N_2 signal is considered between a lower and an upper reference altitude. As described in Whiteman et. al., (2001), if the upper reference altitude for the attenuation calculation is chosen several km above the cloud, the influence of multiple scattering

is greatly reduced. Based on this previous study, if the cirrus cloud optical depth is less than 1 (~85% of the clouds studied here), the influence of multiple scattering on the measurements of optical depth presented here will be less than 5% assuming a 20 micron cloud mean effective particle size and an upper reference altitude that is 5 km above cloud top. The effect of multiple scattering on cirrus clouds was studied here both with multiple scattering modeling (Eloranta, 1998, Whiteman et. al., 2001) for cloud mean particle sizes up to 20 microns and empirically by progressively increasing the upper reference altitude and re-calculating the optical depth. These studies both indicated that the error in optical depth calculation for even the most dense cirrus clouds studied should be less than 10%.

The cloud backscatter coefficient is calculated from the aerosol scattering ratio and the molecular backscatter coefficient as described in Whiteman 2003 a,b., Since this quantity is calculated using the ratio of lidar signals, the influence of multiple scattering on these calculation is minimal (Wandinger, 1998). The cloud mean extinction-to-backscatter ratio is then just the total optical depth divided by the integrated cloud backscatter coefficient.

Cloud base and cloud top were identified using a threshold technique applied to the aerosol scattering ratio, which is formed from the ratio of the backscatter signal and the Raman N_2 signal (Whiteman et. al. 2003 a,b). A scattering ratio value of 2.0 was used to indicate the presence of clouds.

Raman Lidar Measurements of Cirrus Clouds

Raman lidar systems have proven very useful at quantifying cirrus cloud optical depth and extinction-to-backscatter ratio (Ansmann et. al., 1992, Reichardt et. al., 2002, Whiteman et. al. ,

2001) even in the presence of multiple scattering (Eloranta, 1998, Reichardt, 2000, Whiteman et. al., 2001). The unique advantage of a lidar system that measures pure molecular scattering such as a Raman or High Spectral Resolution Lidar (Eloranta, 2000) is that the cirrus cloud extinction-to-backscatter ratio (S in units of sr) can be determined directly without the use of inversion (Klett, 1980). At these wavelengths, S quantifies the ratio of total light scattering to that component of light backscattered to the lidar receiver. Its value is therefore determined by the scattering phase function of the crystals being probed. It is a required parameter for inversion of extinction and optical depth from backscatter lidars that do not measure a pure molecular signal. To our knowledge the current work is the only study of cirrus cloud properties made in a sub-tropical or tropical location using either a Raman or High Spectral Resolution Lidar (HSRL).

Statistics of Cirrus Clouds Measured at Andros Island, Bahamas during CAMEX-3

More than 350 hours of lidar measurements were analyzed for this study. Cirrus clouds were present in approximately 220 hours or approximately 62% of the lidar data. For the period of the CAMEX-3 experiment (August-September, 1998), there were two sources of cirrus cloud generation: 1) thunderstorms that originated in the general vicinity of Andros Island and 2) hurricanes that developed from disturbances off the coast of Africa and intensified as they traveled westward toward the Bahamas. A total of approximately 40 hours of measurements of cirrus cloud analyzed as a part of this study were due to outflow from three hurricanes (Bonnie, Danielle, and Earl). The statistics of the hurricane-induced and non-hurricane induced cirrus clouds have been separately calculated to study the influence of generating mechanism on cirrus properties.

Frequency of occurrence and cloud heights

Figure 1 presents the frequency distributions of cloud base and top heights where the data have been segmented by generating mechanism into hurricane- (red) and non-hurricane- (black) induced. The data are binned in 1 km increments. The maximum frequency of occurrence of cloud top is between 15 and 16 km (12 and 13 km) for hurricane (non-hurricane) conditions. The hurricane-induced cirrus cloud tops peak just below the mean tropopause height, which was observed to be ~16.5 km based on radiosonde analysis whereas for the non-hurricane cases the well-defined peak occurred ~4km below the tropopause. Both the hurricane and non-hurricane cloud top heights are higher than the same summertime statistic at the mid-latitude sites of northern Oklahoma (Wang and Sassen 2002) and Salt Lake City, Utah (Sassen and Campbell 2001) where, in both of these cases, the maximum frequency was between 9-10 km. Interestingly, Sassen and Campbell (2001) found in their mid-latitude data that during the summer months the difference in height of the tropopause and cloud top was broadly distributed between approximately 0.5 and 5.5 km with no significant peak to the distribution. The differences in the shapes of these distributions (the sub-tropical ones studied here and the mid-latitude one from Sassen and Campbell) is likely due to the fact that the mid-latitude cirrus clouds are created both by convection and air mass motion (fronts) giving rise to cirrus at varying altitudes whereas the sub-tropical site is dominated by convectively created cirrus clouds that rise to more consistent heights.

The hurricane-induced cirrus cloud top heights studied here are similar to those observed during April – November at the tropical western pacific site of the Department of Energy's (DOE)

Atmospheric Radiation Measurements (ARM) program (Comstock et al. 2002), where the maximum frequency also occurred between 15-16 km. Figure 1 shows as well that the maximum frequency of occurrence of cloud base was between 12 and 13 km (8 and 9 km) for hurricane (non-hurricane) conditions. For the entire dataset, the cloud tops detected ranged between 7 and 18 km while the cloud bases ranged between 7 and 16 km. The general trend of finding higher cirrus clouds progressing from the mid-latitudes to the tropics is due to the stronger convective storms that are found in tropical and sub-tropical locations versus those in the mid-latitudes.

Cloud optical depths

The frequency distribution of cirrus cloud optical depth for the entire CAMEX-3 dataset is shown in figure 2a where again the data have been segmented into hurricane (red) and non-hurricane (black) induced. For the non-hurricane cases with optical depths below 1 (~85% of the total cases), the frequency of occurrence of optical depth increases nearly exponentially with decreasing optical depth. The frequency of occurrence of optical depths between 1 and 2.5 for these cases is relatively constant and more than an order of magnitude less than for clouds with optical depths below 1. For optical depths above ~3, again there is an exponential decrease with increasing optical depth toward an optical depth of ~4, which is the upper limit of the SRL optical depth measurement capability. For the hurricane-induced cases, the histogram is much more peaked with the maximum frequency of cases occurring with optical depths below 0.2. Figure 2b shows these same data but only for the cases with optical depth below 0.2 revealing that, for all optical depths below 0.2, cirrus clouds are found more frequently in the hurricane-induced dataset than in the non-hurricane dataset. Figure 2c shows the same data as in figure 2b

but now the normalization has been done for optical depths below 0.2. Thus, the integral of both curves shown in figure 2c is 1.0. This figure indicates that the general shape of the frequency distribution for cirrus clouds with optical depth below 0.2 did not differ significantly depending on which generating mechanism was considered.

Based on the data shown in figure 2a, approximately 19% of the clouds had optical depths below 0.05. An optical depth of 0.05 is the value that has been established as the desired cirrus optical depth detection threshold for EOS sensors (King, 1999) but our previous cirrus investigations (Whiteman et. al, 2001) indicate, for example, that GOES satellite is sensitive to the presence of cirrus at optical depth levels as low as 0.005. Furthermore, those same studies indicated approximately a 20% wet bias in the retrieval of total precipitable water from GOES if a cirrus cloud of 0.05 is undetected. In agreement with other studies, the cirrus cloud frequency results presented here imply that a large number of thin cirrus clouds are likely to go undetected by satellite in the sub-tropics potentially causing significant errors in satellite retrievals of water vapor, aerosols and other quantities.

Cloud layer mean extinction

The variation of optical depth and layer mean extinction coefficient with respect to mid-cloud temperature is presented in figure 3. The vertical bars indicate the standard deviation of the data. For comparisons, the temperature dependencies of layer mean extinction coefficient at the Southern Great Plains (SGP) site (Wang and Sassen 2002) and optical depth at the University of Utah Facility for Atmospheric Remote Sensing (FARS), (Sassen and Comstock 2001) are also plotted. The statistics for both of these quantities are similar at these two mid-latitude sites.

Although the non-hurricane layer mean extinction values at a given temperature measured at Andros Island and SGP agree within the standard deviation error bar, the general trend of the measurements is for both the non-hurricane and hurricane cases measured at Andros to have lower layer mean extinction than the cirrus clouds measured at SGP or FARS. Likewise there is a tendency for the optical depths of both the hurricane and non-hurricane cirrus at Andros to possess lower optical depths than those measured at either SGP or FARS. The generally lower mean extinction and optical depths measured at Andros Island could be a seasonal effect created by the increased persistence of cirrus clouds in the moist summer season in the sub-tropics. More extended datasets in the sub-tropics would be needed to assess this possibility.

Extinction-to-backscatter(lidar) ratio, S

The extinction-to-backscatter ratio, S, also known as the lidar ratio, is an important parameter that quantifies optical scattering properties of cirrus particles. It also is a required parameter for inversion of extinction or optical depth from backscatter lidar data if aerosol contamination or multiple scattering effects are present. In order to improve cirrus cloud optical depth retrievals from space-based lidar such as CALIPSO, where multiple scattering effects will be present, it is important to study the dependence of S on such variables as temperature, geographic location and cirrus generation mechanism. Figure 4 presents the frequency distribution of layer mean S for the CAMEX-3 dataset. The mean values of S for the hurricane and non-hurricane data are 19.0 +/- 5.3 and 20.4 +/- 7.5, respectively, indicating no significant difference in mean values depending on generating mechanism. The hurricane data distribution is considerably more

peaked than the non-hurricane data, however, implying that the range of cirrus cloud conditions sampled in the non-hurricane dataset is larger than for the hurricane dataset.

Figure 5 presents the same data as in figure 4, but this time as a function of mid-cloud temperature (a), optical depth (b) and cloud height (c). Here clear differences in S values due to generating mechanism can be observed. For all three comparisons, the non-hurricane induced cirrus clouds possess consistently higher S values than the hurricane cases. Furthermore, the trend in S for decreasing temperature is quite different for these two datasets. For the hurricane cases, S shows a general decrease from approximately 25 to 15 sr for temperatures decreasing from –50 to -70C. The non-hurricane cases show a general increase in S values from approximately 25 to 35 over a similar temperature range. This same trend is reflected in the S versus cloud height data, which is sensible since temperatures tend to decrease with altitude. However, the S versus optical depth data show a similar trend of decreasing S for decreasing optical depth for optical depths below 0.2 in both the hurricane and non-hurricane cases.

It is difficult to offer a definitive explanation for the mean differences observed between the hurricane and non-hurricane S data at the same mid-cloud temperature, optical depth or cloud height. It would seem apparent however that these differences are related to lifetime of the cirrus particles, since for the hurricane data anvil outflows persist for days at a time with the hurricane remaining in contact with it's water source of energy permitting crystals to be regenerated within the outflows (c.f. Sassen et. al., 2003). The non-hurricane cases are due to more local thunderstorms with a shorter life cycle. How this difference in lifetime might explain the differences in the behavior of S for the two generating mechanisms shown in figure 5 is not

known at this time. Nonetheless, whatever the source of the differences in the measured S values from this CAMEX-3 dataset, it is clear that mean extinction to backscatter ratios for cirrus clouds are strongly a function of the method of generation of the cirrus cloud.

It is interesting to compare the values of S versus temperature measured here with others that have been published. Reichardt et al., 2002 studied the temperature and depolarization dependence of S for a selected set of arctic cirrus clouds. Mean S(T) values varied roughly between 10-30 sr in good agreement with the values presented here. Curiously, a decreasing trend in S values was observed for the coldest clouds that they studied much like the hurricane results shown in figure 5a. The explanation for why S(T) for air-mass induced cirrus clouds in the arctic and hurricane-induced ones from the sub-tropics might have similar behavior is not known at this time.

Backscatter lidar studies of cirrus cloud S versus cloud temperature have also been made. Del Guasta (2001) studied S(T) for Antarctic cirrus clouds and showed a generally increasing value of S for decreasing cloud temperature; a trend that generally agrees with the non-hurricane clouds studied here although the magnitudes of their S values are approximately 50% higher than those presented here. Chen et. al.(2002) studied cirrus clouds over Taiwan and show a relationship of S generally decreasing with temperature between –50 and –75C in agreement with our hurricane segmented data. Their values of S are in reasonable agreement with the non-hurricane data shown here near –70C, however at –50C their values are approximately 100% larger than those shown here. Platt et. al. (2002) have published a recent analysis of S(T) based on LIRAD measurements of tropical cirrus clouds near the coast of Australia. Their results indicate S values increasing from approximately 40 to 100 sr over a temperature range of –35 to

-75C. The general increase in S with decreasing temperature agrees with our non-hurricane data, but the values in the Platt study are 2-3 times as large as the values presented here.

Summary and Conclusions

The NASA GSFC Scanning Raman Lidar was stationed on Andros Island in the Bahamas during July – September, 1998 for the CAMEX-3 hurricane study program To our knowledge, these measurements are the only Raman lidar measurements of cirrus clouds from a tropical or sub-tropical location and therefore contribute to the knowledge of the variation in cirrus properties as a function of location (sub-tropics) and season (summertime). The analysis presented here should also be of interest to those involved in cirrus cloud studies from the Cirrus Regional Study of Tropical Anvils and Cirrus Layers – Florida Area Cirrus Experiment (CRYSTAL-FACE), which occurred in south Florida in July, 2002, since our analysis helps to characterize mean cirrus cloud properties in the same region and during the same season as for CRYSTAL-FACE.

The analysis presented here indicates that cirrus clouds occurred in 62% of the more than 350 hours of data analyzed. In addition, 19% of these cirrus clouds possessed optical depths below the EOS cloud detection threshold of 0.05. Cloud base and top statistics were presented and compared with other datasets indicating that mean cloud heights tend to increase from the mid-latitudes toward the tropics. The hurricane induced CAMEX-3 cirrus cloud tops peaked just below the tropopause whereas the non-hurricane induced cirrus clouds peaked approximately 4 km below the tropopause. The dependences of the cirrus cloud extinction to backscatter ratio (S) on temperature, cloud height and optical depth were studied for hurricane and non-hurricane cases. The values of S were consistently lower for the hurricane cases. Comparisons with other

S(T) measurements were made indicating generally good agreement with a previous Raman Lidar study of Reichardt (2002) but showing significant differences (~50%) with S(T) studies based on backscatter lidar (Del Guasta, 2001, Chen, 2002) and very large differences (a factor of 2-3) with the LIRAD technique (Platt 2002).

Knowledge of the variation of S due to factors such as temperature, geographic location, and cirrus generation mechanism is needed to develop cirrus cloud optical depth retrieval algorithms from upcoming space-based lidar systems such as CALIPSO, which will use backscatter measurements to infer cloud and aerosol optical depth through the use of an assumed extinction to backscatter ratio, S. The current study indicates that there is good agreement between two Raman lidar studies of cirrus cloud S values but that there are large disagreements among the other available studies of the temperature dependence of the cirrus cloud extinction to backscatter ratio. These results imply that large uncertainties likely exist in any parameterization of S(T) based on published data. Furthermore, the results presented here indicate that any parameterization should take into account the cirrus cloud generating mechanism to provide an accurate S value for an inversion of optical depth. Simultaneous measurements of cirrus cloud properties using various lidar techniques are called for to address the large differences in S values that have been found in this study and to work toward a more robust parameterization of S for use in space-based cloud optical depth retrievals.

References

1. Ansmann, A., U. Wandinger, M. Riebesell, C. Weitkamp, and W. Michaelis, Independent measurements of extinction and backscatter profiles in cirrus clouds by using a combined Raman elastic-backscatter lidar, *Appl. Opt.*, **31**, 7113-7131, 1992.

2. Comstock, J. M., T. P. Ackerman, and G. G. Mace, Ground based lidar and radar remote sensing of tropical cirrus clouds at Nauru Island: Cloud statistics and radiative impacts, *J. Geophys. Res.*, **107**, 4714, 2002.

3. Chen, W-N., C-W. Chiang, J-B Nee, Lidar ratio and depolarization ratio for cirrus clouds, Appl. Opt., 41, 6470-6476.

4. Del Guasta, N., Simulation of LIDAR returns from pristine and deformed hexagonal ice prosms in cold cirrus clouds by means of "face tracing", *J. Geophys. Res.*, 106, 12,589-12,602, 2001.

5. Eloranta, E. W., Practical model for the calculation of multiply scattered lidar returns, Appl. Opt., **37**, 2464-2472, 1998.

6. Eloranta, E. W., A High Spectral Resolution Lidar for long-term unattended operation in the Arctic, *ARM Science Team Meeting*, San Antonio, Texas. March 2000.

7. Gao, B.-C., Y.J. Kaufman, D. Tanré and R.-R. Li, Distinguishing tropospheric aerosols from thin cirrus clouds for improved aerosol retrievals using the ratio of 1.38-μm and 1.24-μm channels. *Geophys. Res. Lett.*, **29**, 1890, doi:10.1029/2002GL015475, 2002.

8. King, M. D., 1999: EOS Science Plan - The state of science in the EOS program, NASA publication http://eospso.gsfc.nasa.gov/sci_plan/chapters.html.

9. Klett, J. D., Stable analytical inversion solution for processing lidar returns, *Appl. Opt.* , **20**, 211-220, 1981

10. Liou, K.-N., The influence of cirrus on weather and climate processes, A global perspective, *Mon. Wea. Rev.*, **114**, 1167-1199, 1986.

11. Mace, G. G., E. E. Clothiaux, and T. P. Ackerman, The composite characteristics of cirrus clouds: Bulk properties revealed by the one year of continuous cloud radar data, *J. Climate*, **14**, 2185-2203, 2001.

12. McFarquher, G. M., A. J. Heymsfield, J. D. Spinhirne, and Bill Hart, Thin and subvisual tropical cirrus: Observation and radiative impacts, *J. Atmos. Sci.* **57**, 1841-1853, 2000.

13. Platt, C. M. R., J. C. Scott, and A. C. Dilley, Remote sensing of high clouds, Part IV, Optical properties of midlatitude and tropical cirrus, *J. Atmos. Sci.*, **44**, 729-747, 1987.

14. Platt, C. M. R., S. A. Young, P. J. Manson, G. R. Patterson, S. C. Marsden, R. T. Austin, and J. H. Churnside, The optical properties of equatorial cirrus from observations in the ARM Pilot Radiation Observation Experiment, *J. Atmos. Sci.*, **55**, 1977-1996, 1998.

15. Platt., C. M. R., LIRAD Observations of Tropical Cirrus Clouds in MCTEX. Part I: Optical Properties and Detection of Small Particles in Cold Cirrus, J. Atmos. Sci., 59, 3145-3162, 2002.

16. Reichardt, J., M. Hess, and A. Macke, Lidar inelastic multiple-scattering parameters of cirrus particle ensembles determined with geometrical-optics crystal phase functions, *Appl. Opt.* **39**, 1895-1910, 2000.

17. Reichardt, J., S. Reichardt, A. Behrendt, and T. J. McGee, Correlations among the optical properties of cirrus-cloud particles: Implications for spaceborne remote sensing, *Geophys. Res. Lett.*, **29**, 1029-1032, 2002.

18. Sakai, T., T. Nagai, M. Nakazato, Y. Mano, T. Matsumura, Ice clouds and Asian dust studied with lidar measurements of particle extinction-to-backscatter ratio, particle depolarization, and water vapor mixing ratio over Tsukuba, *Appl. Opt.*, **42**, 7103-7116.

19. Sassen, K., R. P. Benson, and J. D. Spinhirne, Tropical cirrus cloud properties derived from TOGA/COARE airborne polarization lidar, *Geophys. Res. Lett.*, **27**, 673-676, 2000.

20. Sassen, K., and J. R. Campbell, A midlatitude cirrus cloud climatology from the facility for atmospheric remote sensing. Part I Macrophysical and synoptic properties, *J. Atmos. Sci.*, **58**, 481-496, 2001.

21. Sassen, K., and J. M. Comstock, A midlatitude cirrus cloud climatology from the facility for atmospheric remote sensing. Part III: Radiative properties, *J. Atmos. Sci.*, **58**, 2113-2127, 2001.

22. Sassen, K. , W. P. Arnott, D. O'C Starr, G. Mace, Z. Wang, M. Poellet, Midlatitude cirrus clouds derived from Hurrican Nora: A case study with implications for ice crystal nucleation and shape, *J. Atmos. Sci.*, **60**, 873-891

23. Wandinger U, Multiple-scattering influence on extinction- and backscatter-coefficient measurements with Raman and high-spectral-resolution lidars Appl. Opt. 37 (3): 417-427 1998.

24. Wang, P.-H., P. Minnis, M. P. McCormick, G. S. Kent, and K. M. Skeens, A 6-year climatology of cloud occurrence frequency from Stratospheric Aerosol and Gas Experiment II observations (1985-1990), *J. Geophys. Res.*, **101**, 29,407-29,429, 1996.

25. Wang, Z., and K. Sassen, Cirrus cloud microphysical property retrieval using lidar and radar measurements. Part II: Midlatitude cirrus microphysical and radiative properties, *J. Atmos. Sci.*, **57**, 2291-2302, 2002.

26. Whiteman, D. N., S. H. Melfi, and R. A. Ferrare, Raman lidar system for measurement of water vapor and aerosols in the Earth's atmosphere", *Appl. Opt.*, **31**, 3068 - 3082 , 1992.

27. Whiteman, D. N., K. D. Evans, B. Demoz, D. O'C Starr, E. W. Eloranta, D. Tobin, W. Feltz, G. J. Jedlovec, S. I. Gutman, G. K. Schwemmer, M. Cadirola, S. H. Melfi, and F. J. Schmidlin, Raman lidar measurements of water vapor and cirrus clouds during the passage of Hurricane Bonnie, *J. Geophys. Res.* **106**, 5211-5225, 2001.

28. Whiteman, D. N., and S. H. Melfi, Cloud liquid water, mean droplet radius, and number density measurements using a Raman lidar, *J. Geophys. Res.*, **104**, 31,411-31,419, 1999.

29. Whiteman, David N., Examination of the traditional Raman lidar technique. I. Evaluating the temperature-dependent lidar equations, *Applied Optics*, **42**, 2571-2592,2003a.

30. Whiteman, David N., Examination of the traditional Raman lidar technique. II. Evaluating the ratios for water vapor and aerosols, *Applied Optics*, **42**, 2593-2608, 2003b.

Figure Captions:

Figure 1. The frequency distributions of cirrus cloud base, cloud top, and tropopause heights from Andros Island, Bahamas based on Raman lidar measurements acquired during July – September, 1998. The data have been segmented by generating mechanism: hurricane induced (red) and thunderstorm induced (black).

Figure 2. a) The frequency distribution of cirrus cloud UV optical depth. The maximum frequency of occurrence is for an optical depth of approximately 0.03. The hurricane data are shown in red and the non-hurricane data in black. b) shows the same data as in a) but for optical depths below 0.2 c) presents the data for optical depths below 0.2 where now the normalization has been performed over the optical depth range of 0 – 0.2.

Figure 3. The temperature dependence of optical depth and layer mean extinction coefficient. For comparisons, similar results from midlatitude sites (SGP: Wang and Sassen 2002; FARS: Sassen and Comstock 2001) are plotted.

Figure 4. Frequency distribution of the extinction to backscatter ratio for the CAMEX-3 hurricane (red) and non-hurricane (black) measurements.

Figure 5. The dependence of S on mid-cloud temperature, optical depth and cloud height are presented here.

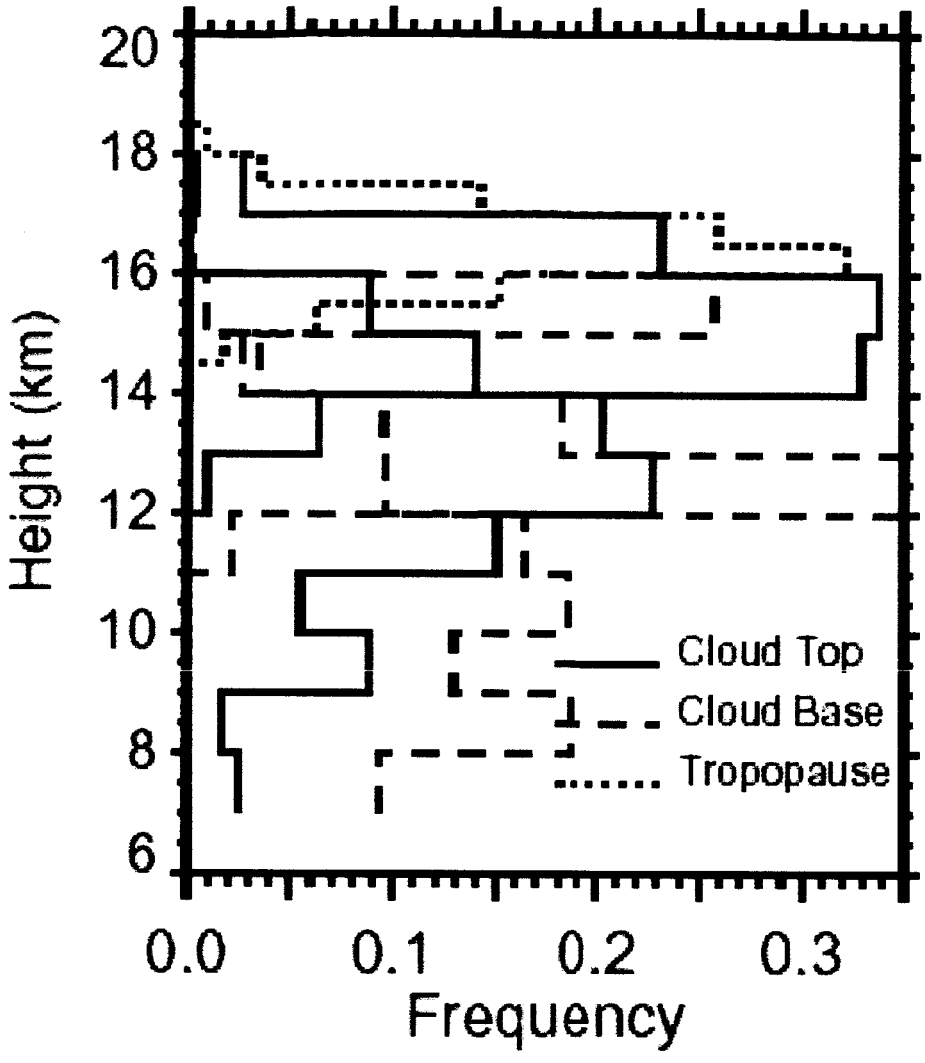
20
18
16
14
12
10
8
6
Height (km)
0.0
0.1
0.2
0.3
Frequency
Cloud Top
Cloud Base
Tropopause

Figure 1

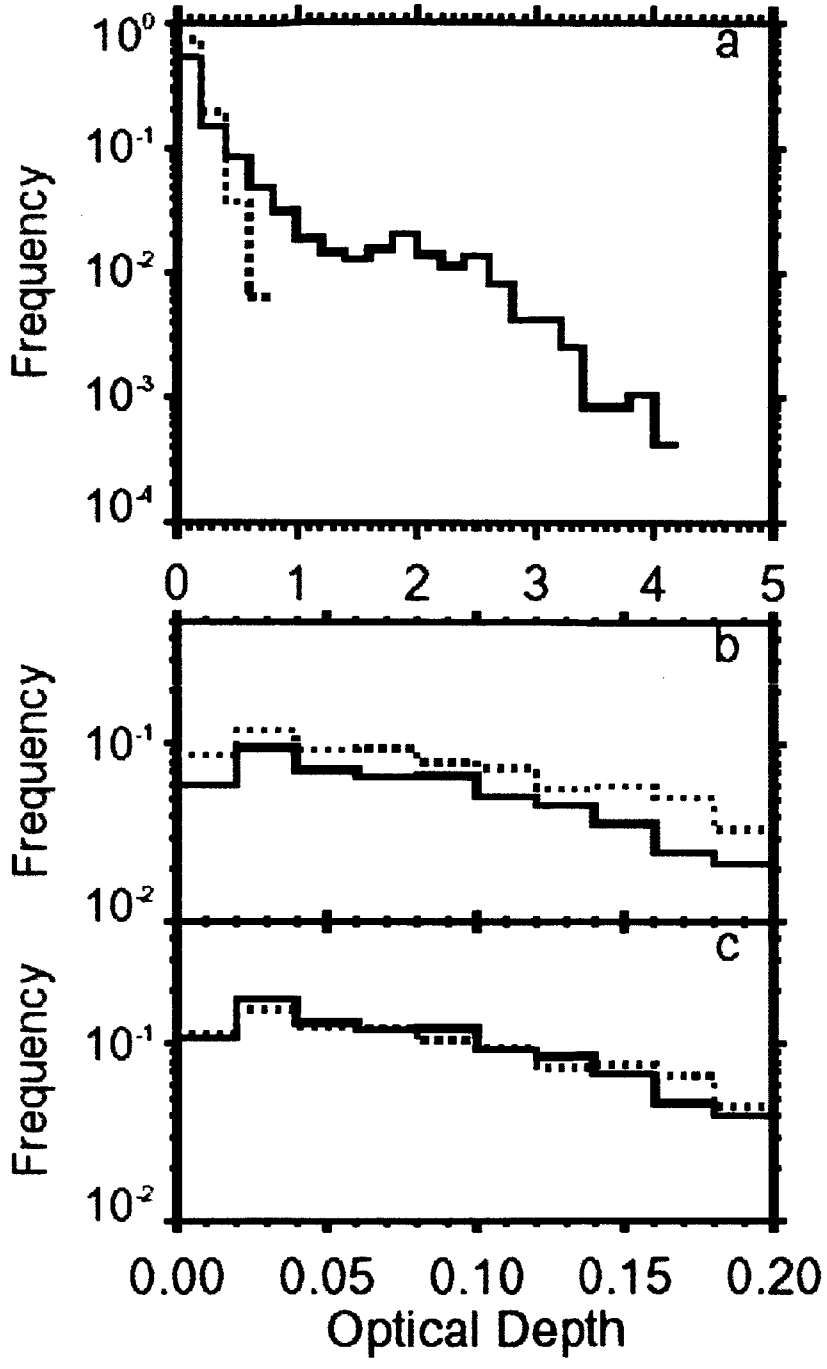
a
b
c
Frequency
Frequency
Frequency
10^{0}
10^{-1}
10^{-2}
10^{-3}
10^{-4}
0
1
2
3
4
5
10^{-1}
10^{-2}
10^{-1}
10^{-2}
0.00
0.05
0.10
0.15
0.20
Optical Depth

Figure 2

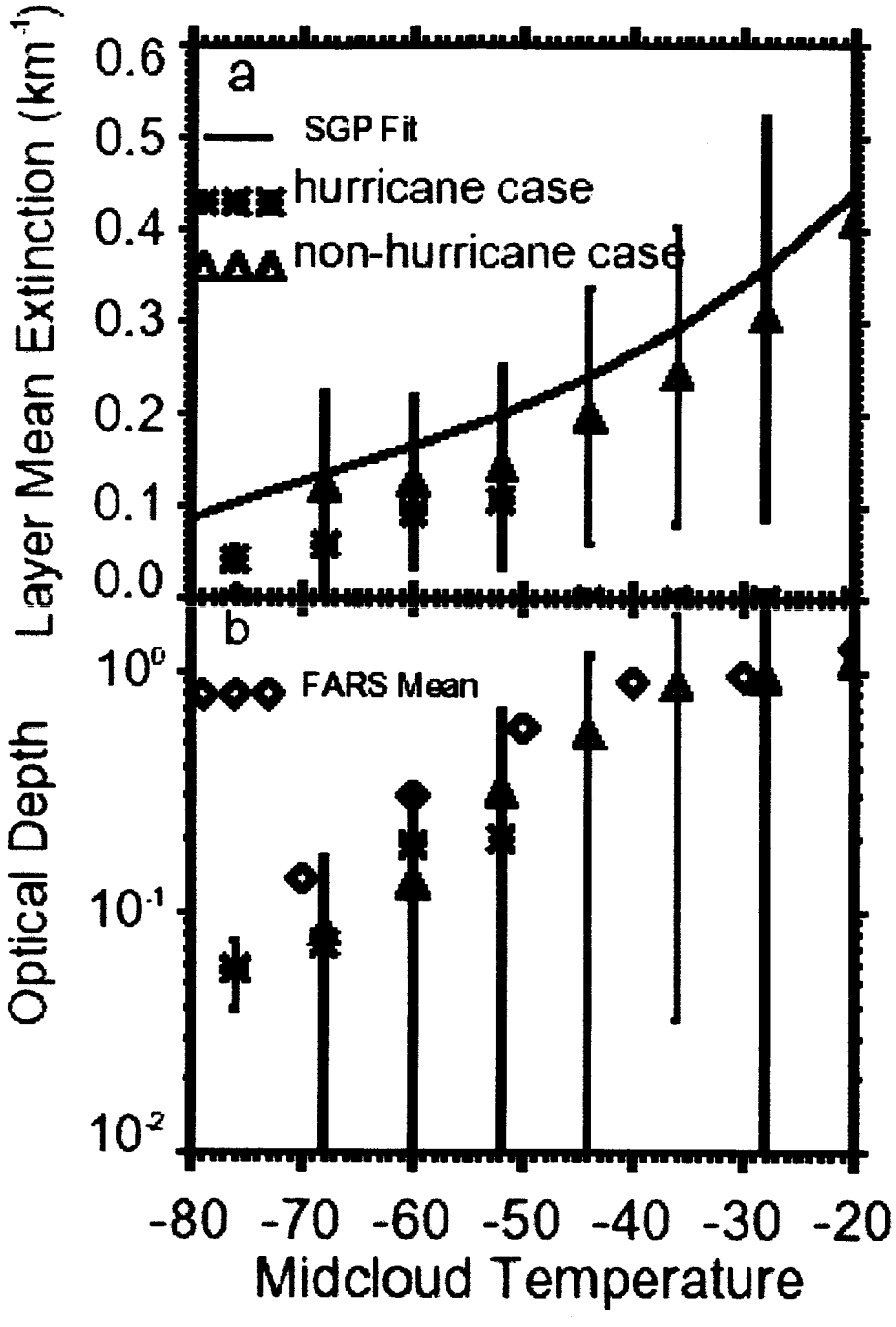
Optical Depth Layer Mean Extinction (km-1)
0.6
0.5
0.4
0.3
0.2
0.1
0.0
a
SGP Fit
hurricane case
non-hurricane case
b
10^0
FARS Mean
10^-1
10^-2
-80 -70 -60 -50 -40 -30 -20
Midcloud Temperature

Figure 3

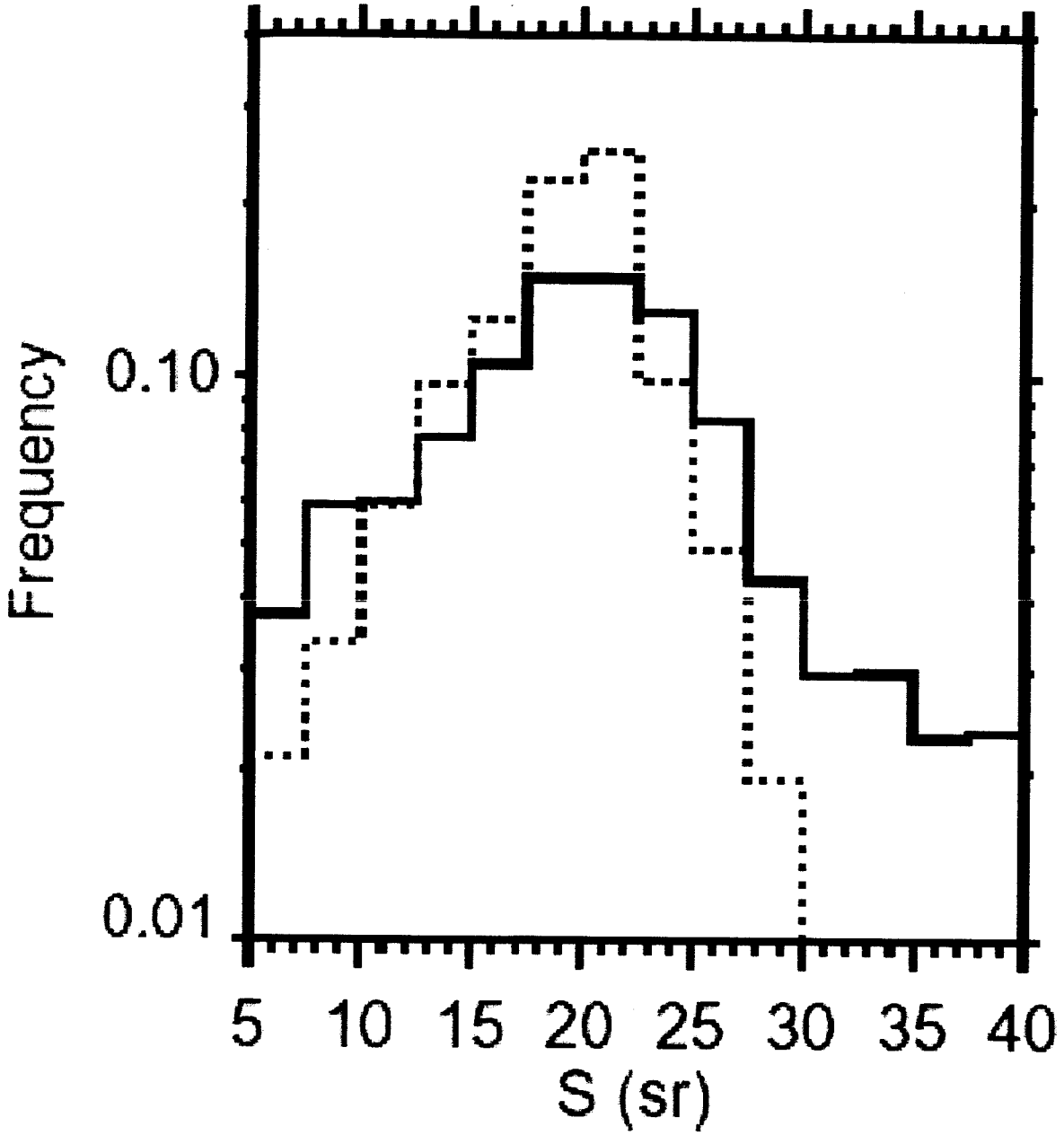

Figure 4

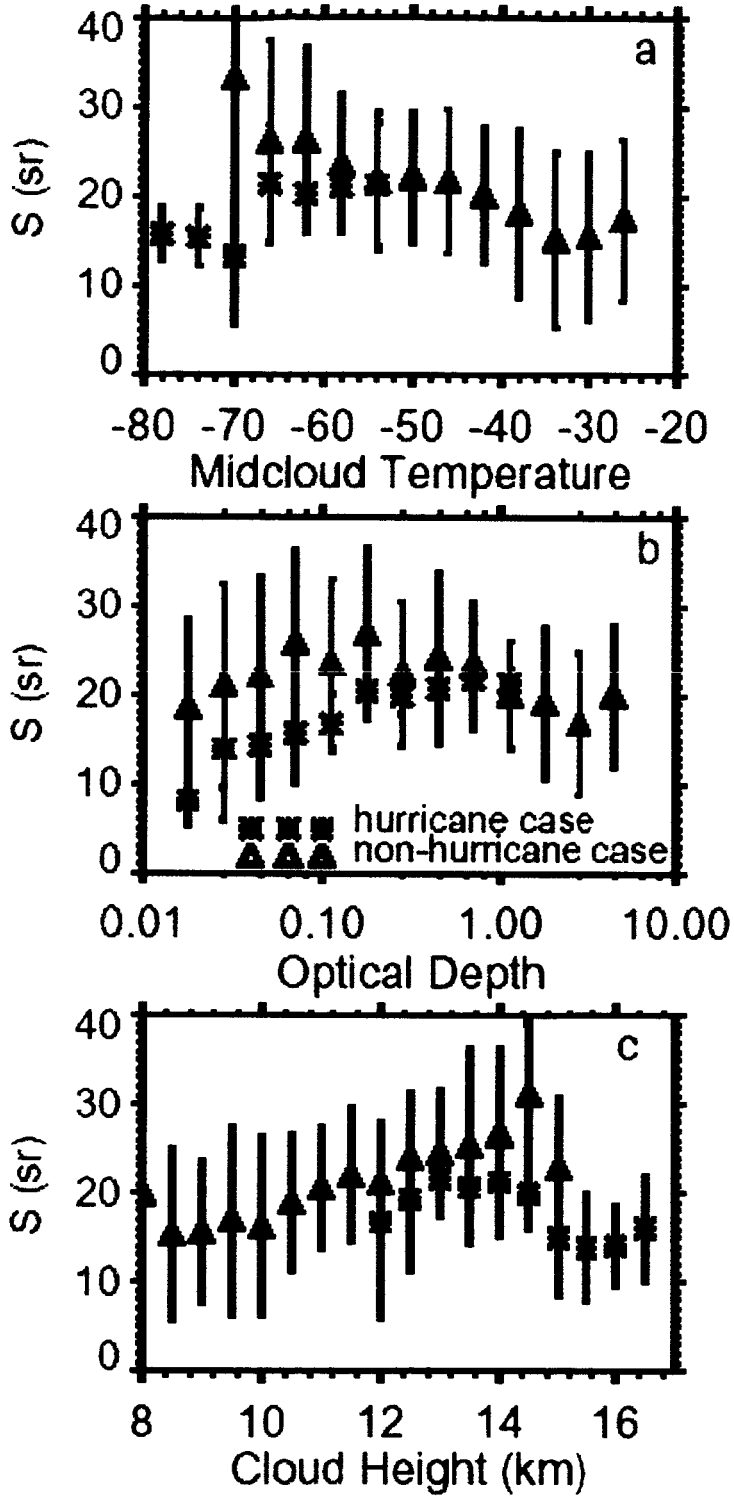
a
S (sr)
40
30
20
10
0
-80 -70 -60 -50 -40 -30 -20
Midcloud Temperature
b
S (sr)
hurricane case
non-hurricane case
0.01 0.10 1.00 10.00
Optical Depth
c
S (sr)
8 10 12 14 16
Cloud Height (km)

Figure 5